Microscopic study of $M1$ resonances in Sn isotopes

Shuai Sun,[1,2] Li-Gang Cao ®,[1,2,*] Feng-Shou Zhang ®,[1,2,3,†] Hiroyuki Sagawa,[4,5] and Gianluca Colò ®[6]

[1]*Key Laboratory of Beam Technology of Ministry of Education, College of Nuclear Science and Technology,*
Beijing Normal University, Beijing 100875, China
[2]*Institute of Radiation Technology, Beijing Academy of Science and Technology, Beijing 100875, China*
[3]*Center of Theoretical Nuclear Physics, National Laboratory of Heavy Ion Accelerator of Lanzhou, Lanzhou 730000, China*
[4]*RIKEN Nishina Center, Wako 351-0198, Japan*
[5]*Center for Mathematics and Physics, University of Aizu, Aizu-Wakamatsu 965-8560, Japan*
[6]*Dipartimento di Fisica, Università degli Studi di Milano, and INFN, Sezione di Milano, Via Celoria 16, 20133 Milano, Italy*

The magnetic dipole ($M1$) resonances of even-even $^{112-120,124}$Sn isotopes are investigated in the framework of the self-consistent Skyrme Hartree-Fock + Bardeen-Cooper-Schrieffer (HF+BCS) and quasiparticle random phase approximation (QRPA). The Skyrme energy density functionals SLy5 and T11 with and without tensor terms are adopted in our calculations. The mixed type pairing interaction is used to take care of the pairing effect for open-shell nuclei both in the ground and excited states calculations. The calculated magnetic dipole strengths are compared with available experimental data. The QRPA results calculated by SLy5 and T11 with tensor force show a better agreement with the experimental data than those without the tensor force. By analyzing the HF and QRPA strength distributions of ^{112}Sn and ^{124}Sn, we discuss the effect of tensor force on the $M1$ resonances in detail. It is found that the $M1$ resonance is sensitive to the tensor interaction, and favors especially a negative triplet-odd tensor one. Depending on the nucleus, a quenching factor of the $M1$ operator of about 0.71–0.95 is needed to reproduce the total observed transition strength. In our calculations, we also find some low-lying, pygmy-type magnetic dipole states distributed below 6.0 MeV, and they are formed mainly from the neutron configuration $\nu 2d_{5/2} \rightarrow \nu 2d_{3/2}$.

I. INTRODUCTION

The magnetic dipole ($M1$) resonance is one of the fundamental excitations of spin-flip type in finite nuclei [1–5]. It has been studied experimentally and theoretically for several decades. The $M1$ resonance is known experimentally to include two major components. One is an orbital component at low excitation energy. It is found in deformed nuclei and called scissors mode. In spherical nuclei, the scissors mode is much suppressed. The other spin-flip component is found at an energy of around 8 MeV, contributing to most of the $M1$ strength. The scissors mode in deformed nuclei is interpreted as neutrons and protons vibrating with a small angle with respect to each other in a scissors-like motion, while the higher energy component describes a resonance-like structure made of proton and neutron spin-flip excitations. The study of $M1$ resonance is of great interest not only for the nuclear structure but also for nuclear astrophysics. It provides, in addition to charge-exchange modes, an alternative chance to explore the nuclear interactions in spin and spin-isospin channels and can offer crucial information on nuclear structure [6]. The properties of the $M1$ resonance may impact the description of neutral current neutrino interactions in supernova [7,8],

or the estimate of the reaction cross sections in large-scale nucleosynthesis network calculations [9–11].

In the past years, great efforts have been devoted to the study of $M1$ resonance in the framework of nonrelativistic random phase approximation (RPA) with Skyrme or Gogny interactions, relativistic RPA, and shell model calculations. In the nonrelativistic approaches, it is well known that the distribution of $M1$ resonance is very sensitive to the spin-dependent interactions. So, many studies have focused on the effect of spin-orbit and tensor interactions on the $M1$ strength distribution [10–18]. Recently, the self-consistent description of magnetic dipole resonance with relativistic energy density functionals has become available [19–22]. The density-dependent point-coupling or density-dependent meson exchange interactions are adopted in the calculations. To properly describe the unnatural-parity $M1$ resonance, the isovector-pseudovector interaction should be included in the residual interaction. In the case of the shell model calculations, the studies of the magnetic dipole resonance pay attention to the strengths at low energy for some selected nuclei [23–25].

Experimentally, the magnetic dipole resonance can be excited by inelastic scattering of protons, electrons, and photons, it has been investigated for many years, and a rich amount of database has been built [1–5,26–30]. Recently, electric and magnetic dipole responses along the even-even tin isotopes have been measured in an inelastic proton scattering

*Corresponding author: caolg@bnu.edu.cn
†Corresponding author: fszhang@bnu.edu.cn

experiment at Research Center for Nuclear Physics (RCNP) Osaka University [31,32]. Total photoabsorption cross sections have been derived from the $E1$ and $M1$ strength distributions and show significant differences compared to those from previous experiments. The magnetic dipole strengths in $^{112-120,124}$Sn exhibit a broad distribution between 6 and 12 MeV in all studied nuclei. The new magnetic dipole data in Sn isotopes provide a good opportunity to check the ability of existing nuclear energy density functionals (EDFs) to reproduce the data. In Ref. [21], the authors have investigated $M1$ transitions in even-even $^{100-140}$Sn isotopes based on the relativistic EDFs, by raising many points for discussion. Up to now, a systematic investigation of the new database by nonrelativistic models is still missing.

As we know, the tensor force plays a significant role in nuclear structure studies [33]. The shell evolution of the single-particle energies in some exotic nuclei can be well explained by the inclusion of tensor force [34–42]. Extensive efforts have also been undertaken to study the influence of the tensor force on the excited state properties of finite nuclei, like the spin and spin-isospin excitation modes [43–49]. The tensor force also plays a role in the calculations of the response functions of infinite nuclear matter [50–52]. The effect of the tensor force on heavy-ion collisions has been discussed within the time-dependent Hartree-Fock (TDHF) method. It plays a non-negligible role in dynamic processes in nuclei [53–55]. In this work, we will investigate the $M1$ resonances in even-even $^{112-120,124}$Sn isotopes within the framework of Skyrme Hartree-Fock + Bardeen-Cooper-Schrieffer (HF+BCS) plus quasiparticle RPA (QRPA). The calculated results are compared to the experimental data from Refs. [31,32]. The effect of the tensor force on $M1$ resonances in even-even $^{112-120,124}$Sn isotopes is discussed in detail in the present work. We will also pay attention to the quenching associated with the magnetic dipole operator, which is a longstanding problem in nuclear structure [56–58].

This article is organized as follows. The theoretical model is briefly reviewed in Sec. II. In Sec. III, the calculated results are compared with experimental data. The discussions on the effect of tensor force and quenching problem are also given in Sec. III. The summary and some perspectives for future work are given in Sec. IV.

II. THEORETICAL FRAMEWORK

In this work, a HF + BCS plus QRPA approach is employed in the calculations. Since the theoretical framework of HF + BCS method is well known in the literature (cf. Refs. [59,60]), we briefly review only the QRPA main equations. The matrix equations of QRPA can be written as

$$
\begin{pmatrix} A & B \\ -B^* & -A^* \end{pmatrix} \begin{pmatrix} X^\nu \\ Y^\nu \end{pmatrix} = E_\nu \begin{pmatrix} X^\nu \\ Y^\nu \end{pmatrix}, \tag{1}
$$

where E_ν is the eigenvalue of the νth QRPA state and X^ν, Y^ν are the corresponding forward and backward quasiparticle amplitudes, respectively. The details about the matrix elements A and B can be found in Refs. [61,62].

The magnetic dipole operator is given by

$$
\hat{F}(M1) = \mu_N \sum_{i=1}^{A} (g_l \vec{l}_i + g_s \vec{s}_i) = \mu_N \sum_{i=1}^{A} [g_l \vec{j}_i + (g_s - g_l)\vec{s}_i], \tag{2}
$$

where $\mu_N = e\hbar/2mc$ is the nuclear magneton. Since j is a good quantum number for the single-particle states in spherical nuclei, the first term $g_l \vec{j}_i$ does not contribute to the transition matrix for the p-h type excitation since $j_p \neq j_h$. On the other hand, in open shell nuclei, the two quasiparticle excitation with the same j quantum number, $j_1 = j_2$, contributes to the matrix element. We should notice that even in the p-h type excitation, the orbital contribution exists and it is absorbed in the g factor of spin operator $g_s \rightarrow g_s - g_l$.

For the magnetic dipole operator, the reduced transition strength from the ground state to the excited state ν is written as

$$
\begin{aligned}
B^\nu(M1) &= \frac{1}{2J+1} |\langle \nu || \hat{F} || g.s.\rangle|^2 \\
&= \frac{1}{2J+1} \left| \sum_{c \geqslant d} (X_{cd}^\nu + Y_{cd}^\nu)(v_c u_d + u_c v_d)\langle c \| \hat{F} \| d \rangle \right|^2.
\end{aligned} \tag{3}
$$

In the figures, the $M1$ discrete spectra are convoluted with Lorentzian distributions

$$
S_{M1}(E) = \sum_\nu B^\nu(M1) \frac{1}{\pi} \frac{\Gamma/2}{(E - E_\nu)^2 + \Gamma^2/4}, \tag{4}
$$

where Γ is the width and is taken equal to 2 MeV in present calculations.

The triplet-even and triplet-odd zero-range tensor terms of the Skyrme force are expressed as

$$
\begin{aligned}
v_T = {} & \frac{T}{2} \left\{ \left[(\boldsymbol{\sigma}_1 \cdot \mathbf{k}')(\boldsymbol{\sigma}_2 \cdot \mathbf{k}') - \frac{1}{3}(\boldsymbol{\sigma}_1 \cdot \boldsymbol{\sigma}_2)\mathbf{k}'^2 \right] \delta(\mathbf{r}_1 - \mathbf{r}_2) + \delta(\mathbf{r}_1 - \mathbf{r}_2) \left[(\boldsymbol{\sigma}_1 \cdot \mathbf{k})(\boldsymbol{\sigma}_2 \cdot \mathbf{k}) - \frac{1}{3}(\boldsymbol{\sigma}_1 \cdot \boldsymbol{\sigma}_2)\mathbf{k}^2 \right] \right\} \\
& + U \left\{ (\boldsymbol{\sigma}_1 \cdot \mathbf{k}')\delta(\mathbf{r}_1 - \mathbf{r}_2)(\boldsymbol{\sigma}_2 \cdot \mathbf{k}) - \frac{1}{3}(\boldsymbol{\sigma}_1 \cdot \boldsymbol{\sigma}_2)\mathbf{k}' \cdot \delta(\mathbf{r}_1 - \mathbf{r}_2)\mathbf{k} \right\},
\end{aligned} \tag{5}
$$

where the operator $\mathbf{k} = (\nabla_1 - \nabla_2)/2i$ acts on the right and $\mathbf{k}' = -(\nabla_1 - \nabla_2)/2i$ acts on the left. The coupling constants

T and U denote the strengths of the triplet-even and triplet-odd tensor interactions, respectively.

It is known that the tensor force affects the spin-orbit mean potential. The spin-orbit potential is expressed as

$$V_{\text{s.o.}}^{(q)} = U_{\text{s.o.}}^{(q)} \mathbf{l} \cdot \mathbf{s} \qquad (6)$$

and

$$U_{\text{s.o.}}^{(q)} = \frac{W_0}{2r}\left(2\frac{d\rho_q}{dr} + \frac{d\rho_{1-q}}{dr}\right) + \left(\alpha\frac{J_q}{r} + \beta\frac{J_{1-q}}{r}\right), \qquad (7)$$

where $q = 0(1)$ is the quantum number $(1 - t_z)/2$ (t_z being the third isospin component) that distinguishes neutrons and protons. The first term on the right comes from the Skyrme spin-orbit interaction, and the second term, contributions from J terms, comes from some exchange terms of the central force as well as from the tensor force. The spin-orbit density $\mathbf{J}$ in spherical nuclei has only a radial component whose expression reads

$$J_q = \frac{1}{4\pi r^3}\sum_i v_i^2 (2j_i + 1)\left[j_i(j_i + 1) - l_i(l_i + 1) - \frac{3}{4}\right]R_i^2(r), \qquad (8)$$

where $i = n, l, j$ runs over all states. The quantity v_i^2 is the occupation probability of each orbit determined by the BCS approximation and $R_i(r)$ is the radial part of the HF single-particle wave function. α and β in Eq. (7) include both the central exchange terms and the tensor terms, that is, $\alpha = \alpha_C + \alpha_T$ and $\beta = \beta_C + \beta_T$. The central exchange contributions are written in terms of the usual Skyrme parameters

$$\alpha_C = \frac{1}{8}(t_1 - t_2) - \frac{1}{8}(t_1 x_1 + t_2 x_2),$$
$$\beta_C = -\frac{1}{8}(t_1 x_1 + t_2 x_2), \qquad (9)$$

while the tensor contributions are expressed as

$$\alpha_T = \frac{5}{12}U, \quad \beta_T = \frac{5}{24}(T + U). \qquad (10)$$

In the HF + BCS plus QRPA calculations, we take an effective density-dependent zero-range pairing interaction,

$$V_{\text{pair}}(\mathbf{r}_1, \mathbf{r}_2) = V_0\left[1 - \eta\left(\frac{\rho(\mathbf{r})}{\rho_0}\right)\right]\delta(\mathbf{r}_1 - \mathbf{r}_2), \qquad (11)$$

where $\rho(\mathbf{r})$ is the particle density, and $\rho_0 = 0.16$ fm^{-3} is the density at nuclear saturation. The parameter η represents the pairing type. When η is either 1.0, 0.5, or 0.0, it means a surface, mixed or volume pairing interaction. The mixed pairing interaction is used in our calculations, as it is very effective in describing many properties of finite nuclei [63–65]. The pairing strength V_0 is adjusted to reproduce the empirical neutron gap in ^{120}Sn ($\Delta_n = 1.392$ MeV). Then the same value is adopted for the calculations of other Sn isotopes.

In order to investigate the effect of pairing on the $M1$ strength distribution, as an example, the filling approximation [66,67] and QRPA calculations are performed for ^{120}Sn using SLy5 with tensor force, and the results are shown in Fig. 1. In the filling approximation, pairing is neglected completely, that is, the p-p interaction is also dropped in the QRPA matrix. The $M1$ strength distribution given by the filling approximation shows a unimodal structure with a peak at energy around 9.6 MeV, which is mainly coming from the proton configuration $\pi 1g_{9/2} \to \pi 1g_{7/2}$. In the QRPA result, the main peak is shifted downward to 9.2 MeV. Besides the $M1$ main
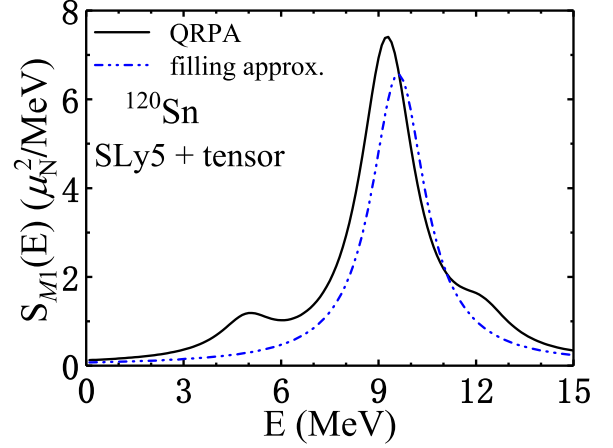

FIG. 1. The $M1$ strength distributions of ^{120}Sn in filling approximation and QRPA, respectively. The calculated strengths are convoluted by a Lorentzian shape with a width of 2.0 MeV.

peak, two additional $M1$ pygmy resonance states emerge at energies around 5.0 and 12.3 MeV, respectively. The word *pygmy state* is often used for a low-lying $E1$ state with smaller strength than giant dipole resonances. On the other hand, many authors employ this word without implying any special multipole, but just referring to the fact that the strength is smaller with respect to giant resonances [68]. Thus it can be used even for low-lying $M1$ or other multipoles. We find that the low-lying state comes from the neutron quasiparticle configuration $\nu 2d_{5/2} \to \nu 2d_{3/2}$ while the high-energy state is due to the $\nu 1h_{11/2} \to \nu 1h_{9/2}$ neutron quasiparticle configuration. The discrepancy between the results of filling approximation and QRPA stems from the particles scattering around the Fermi surface, i.e., the neutron state $2d_{3/2}$ changes from fully occupied to partially occupied, while the neutron $1h_{11/2}$ state turns from being empty to being partially filled. Notice that the states $2d_{5/2}$ and $2d_{3/2}$ are below the Fermi level while $1h_{11/2}$ and $1h_{9/2}$ are above that. These changes by the pairing correlations allow the relatively strong transitions from $\nu 2d_{5/2}$ to $\nu 2d_{3/2}$ and $\nu 1h_{11/2}$ to $\nu 1h_{9/2}$. The above discussion shows that the effect of pairing on the $M1$ resonance is substantial and make appreciable difference from the filling approximation.

III. RESULTS AND DISCUSSIONS

In the present study, all the calculations assume a spherical shape for the even-even Sn isotopes. The quasiparticle states are obtained by solving HF + BCS in coordinate space with a box boundary condition and the size of the box is 24 fm. We have checked that the predicted ground state properties of Sn isotopes, such as binding energies, charge radii, agree well with the experimental data. After solving the HF + BCS equation in coordinate space, we build up a model space of two-quasiparticle configurations for $M1$ excitation, and then we solve the QRPA matrix equations in the model space. The major shell configurations up to $\Delta N = 8$ are adopted to build up the QRPA model space, which is large enough to allow the convergence of the results.
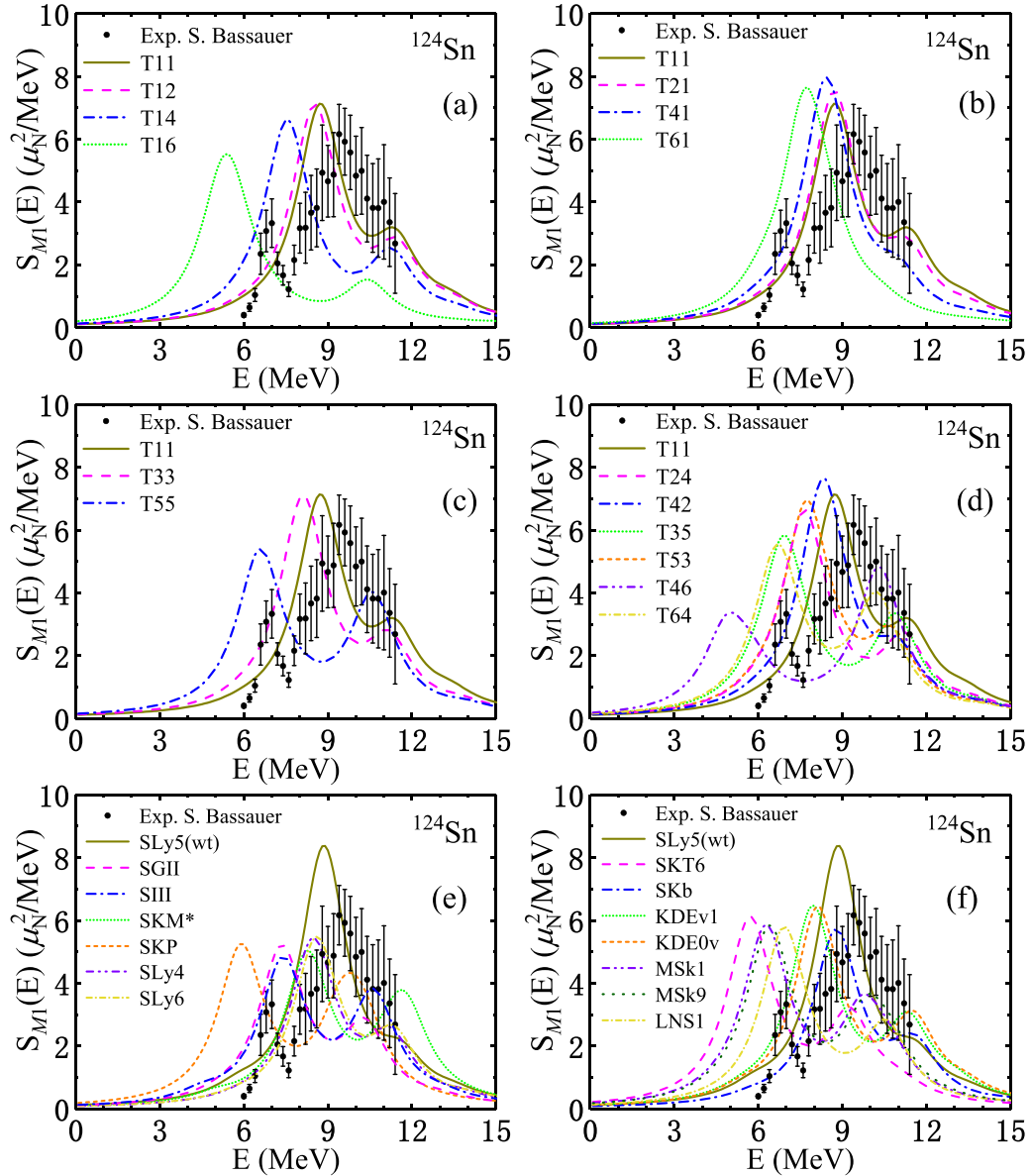
FIG. 2. The QRPA strength distributions of ^{124}Sn calculated by using several Tij and other Skyrme EDFs. In (a)–(d), the Tij EDFs are employed: (a) by changing α for a fixed value $\beta = -60$ MeV fm^5. (b) by changing β for a fixed value $\alpha = -60$ MeV fm^5. (c) by fixing $\alpha = \beta = (-60, 60, 180)$ MeV fm^5 that corresponds to $i = j = (1, 3, 5)$. (d) for the cases $\alpha \neq \beta$ that are not shown in (a)–(c), including T24, T42, T35, T53, T46, and T64, except T11. (e) and (f) show commonly used Skyrme EDFs without the tensor terms, except SLy5 which includes the tensor terms. Experimental data are taken from Bassauer *et al.* [32].

A. Skyrme interactions for $M1$

We adopt various commonly used Skyrme EDFs for the $M1$ calculations of ^{124}Sn to examine both the model dependence and the role of tensor interaction. The adopted Skyrme EDFs with tensor terms are SLy5 with the tensor force [36] and some of the Tij interactions [40]. As representatives without the tensor terms, we employ SLy4 and SLy6 [69], SIII [70], SGII [71], SkM* [72], SkP [73], KDE0v and KDEv1 [74], SkT6 [75], MSK1 [76], MSK9 [77], SKb [78], and LNS1 [79] interactions. The calculated and experimental strength distributions are shown in Fig. 2. Figure 2(a) [Fig. 2(b)] shows the results of Tij family specified by T1j (Ti1) sets, in which

the indices i and j refer to the coefficients of the proton-neutron (β) and like-particle (α) spin-orbit densities in Eq. (7),

$$\alpha = \alpha_C + \alpha_T = 60 \, (j - 2) \, \text{MeV fm}^5,$$
$$\beta = \beta_C + \beta_T = 60 \, (i - 2) \, \text{MeV fm}^5. \tag{12}$$

These Tij family members are chosen to investigate the evolution of the strength distributions by increasing the α (β) value at a given β (α) value. Figure 2(c) shows results of the T11, T33, and T55 sets, which are chosen to investigate the strength evolution given by the parameter sets of the $i = j$ family members. Figure 2(d) shows the results of other Tij

parameter sets, including T24, T42, T35, T53, T46, and T64. The results of other Skyrme EDFs without the tensor terms (except SLy5 with the tensor) are shown in Fig. 2(e) and 2(f).

The protocols for the determination of these Skyrme EDFs are as follows. SLy5 is a Skyrme EDF given by Lyon group, and the detailed information can be found in Ref. [69]. The list of constraints used to construct the cost function χ^2 for the minimization reads: the binding energies and the charge radii of ^{16}O, ^{40,48}Ca, ^{56}Ni, ^{132}Sn, and ^{208}Pb; the spin-orbit splitting of the neutron $3p$ state in ^{208}Pb; the energy per particle in the nuclear matter ($E/A \simeq -16$ MeV) at the saturation density ($\rho_0 \simeq 0.16$ fm^{-3}), the incompressibility modulus ($K_\infty \simeq 230$ MeV), and the symmetry energy coefficient ($a_s \simeq 32$ MeV) at the saturation density of nuclear matter; the equation of state of neutron matter predicted by Wiringa *et al.* in Ref. [80]; the enhancement factor κ of the Thomas-Reiche-Kuhn sum rule ($\kappa = 0.25$); x_2 was fixed to be -1.0. The SLy5 functional can be considered as a "standard" Skyrme functional that performs well for many observables like masses, natural parity non-charge-exchange excitations, predictions of drip lines, and the structure of neutron stars. It is employed here as a benchmark of what can be obtained for $M1$ while the fit of the EDF has not been focused on spin properties. Later, Colò *et al.* included the tensor terms perturbatively in the SLy5 interaction in order to reproduce the evolutions of single-particle energies of $Z = 50$ isotopes and $N = 82$ isotones [36].

The Tij parametrizations were proposed in Ref. [40], where indices i and j refer to the proton-neutron (β) and like-particle (α) coupling constants given in Eq. (12). The fit protocol of Tij sets is similar to that of the SLy5 parametrization, but has three differences: (a) the values for α and β were fixed beforehand for each Tij member and then other parameters were optimized for the protocol. This means that the tensor terms were excluded in the fit procedure but fixed *a priori*; (b) the binding energies of ^{90}Zr and ^{100}Sn were added to the set of data; (c) the constraint $x_2 = -1$ imposed on the SLy5 parametrization was released and the parameter x_2 had been included in the optimization process. By using these Tij EDFs, we aim at pinpointing the specific effect of tensor terms on $M1$: since tensor terms affect the spin-orbit splitting, the effect of the point (a) on $M1$ is clear, while (b) and (c) are to some extent details that do not matter too much in the present context.

B. Correlations between $M1$ unperturbed energies and the spin-orbit strength W_0 as well as the tensor terms

In order to clarify the role of the tensor terms of the Skyrme EDFs, we study first the correlation between the unperturbed energies of $M1$ states and the spin-orbit strength W_0 in the case of ^{124}Sn. When the tensor force is not involved, it is expected that the spin-orbit splitting is mainly governed by the spin-orbit strength W_0 together with some contributions from α_C and β_C in Eq. (9). Since the $M1$ unperturbed excitation energy is mainly given by the *p-h* type excitation between the spin-orbit partners, the excitation energies of $M1$ peaks are sensitive to the spin-orbit strength W_0. In Fig. 3, we show the unperturbed low-lying and high-lying $M1$ states for 50 different Skyrme EDFs. There are two main unperturbed
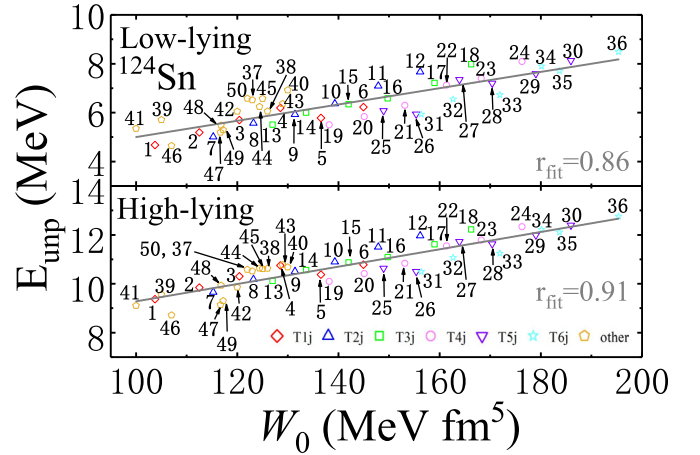

FIG. 3. The energies of unperturbed $M1$ peaks for ^{124}Sn as a function of W_0. In the calculations, the Skyrme EDFs without tensor terms are employed. The computed data points are labeled, here and in what follows, by numbers: 1 = T11, 2 = T12, 3 = T13, 4 = T14, 5 = T15, 6 = T16, 7 = T21, 8 = T22, 9 = T23, 10 = T24, 11 = T25, 12 = T26, 13 = T31, 14 = T32, 15 = T33, 16 = T34, 17 = T35, 18 = T36, 19 = T41, 20 = T42, 21 = T43, 22 = T44, 23 = T45, 24 = T46, 25 = T51, 26 = T52, 27 = T53, 28 = T54, 29 = T55, 30 = T56, 31 = T61, 32 = T62, 33 = T63, 34 = T64, 35 = T65, 36 = T66, 37 = SLy4, 38 = SLy5, 39 = SGII, 40 = SKM*, 41 = SKP, 42 = SIII, 43 = KDE0v, 44 = KDEv1, 45 = SKb, 46 = SKT6, 47 = MSK1, 48 = LNS1, 49 = MSK9, 50 = SLy6. The grey lines correspond to the results of the linear fits.

configurations in ^{124}Sn: the proton configuration $1g_{9/2} \rightarrow 1g_{7/2}$ and the neutron one $1h_{11/2} \rightarrow 1h_{9/2}$. The former corresponds to the low-lying $M1$ state, while the latter corresponds to the high-lying one. As displayed in Fig. 3, it is found that there are clear linear correlations between the energies of unperturbed $M1$ peaks and W_0. The correlation coefficients are $r_{fit} = 0.86$ and 0.91 for the low-lying and high-lying states, respectively.
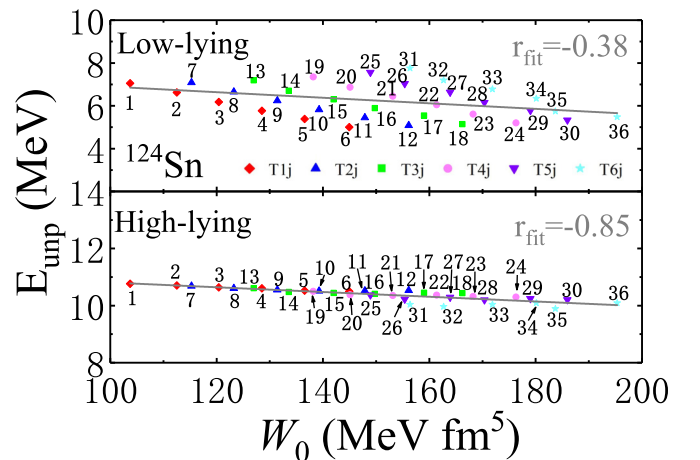

FIG. 4. The energies of low-lying and high-lying unperturbed $M1$ peaks for ^{124}Sn as a function of W_0, calculated by using Tij sets with tensor force.
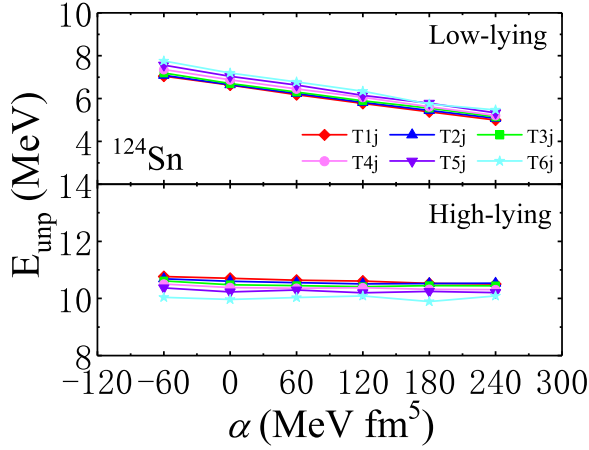
FIG. 5. The energies of low-lying and high-lying unperturbed $M1$ peaks for ^{124}Sn are shown as a function of α by fixing β.

FIG. 7. The difference of the centroid energies of the QRPA and unperturbed response for ^{124}Sn as a function of $G_0 + G_0'$. All sets of Tij family members and other Skyrme forces are adopted in the QRPA calculations. The grey line corresponds to the result of linear fit.

Next we demonstrate what happens in the case of EDFs with tensor terms, i.e., for the Tij family. The W_0 dependence of the energies of low-lying and high-lying $M1$ states is shown for all the parameter sets of the Tij family in Fig. 4. Here, we do not see any clear correlation between the energies and the spin-orbit coupling strength W_0, in contrast to Fig. 3. Curiously, even a weak anticorrelation between the energies and W_0 appears in Fig. 4. This is because the spin-orbit splitting of the like-particle has two contributions, from W_0 and the like-particle spin-orbit density weighted by α in Eq. (7). In the optimization process, the value W_0 is optimized for a given α value to reproduce the empirical spin-orbit splitting in the protocol. Because of this cross-talk feature of W_0 and α, the results of the $M1$ energies do not show any linear dependence with positive slope on W_0.

We have also calculated how the excitation energies of the unperturbed $M1$ peaks depend on the strength of the tensor terms, α or β. We find an anticorrelation between α and the energies of the low-lying $M1$ states, as shown in Fig. 5, but a very weak correlation between the $M1$ energies and β. The anticorrelation on α is due to the feature of this like-particle term, which has an opposite sign with respect to the spin-orbit
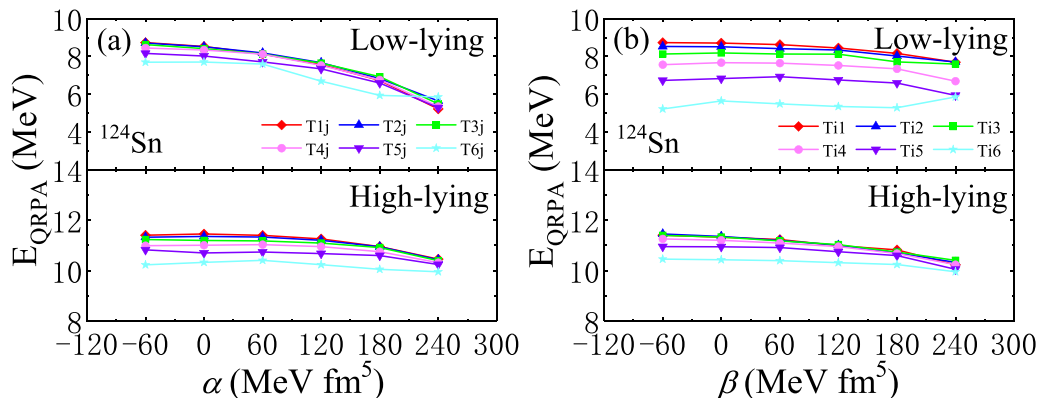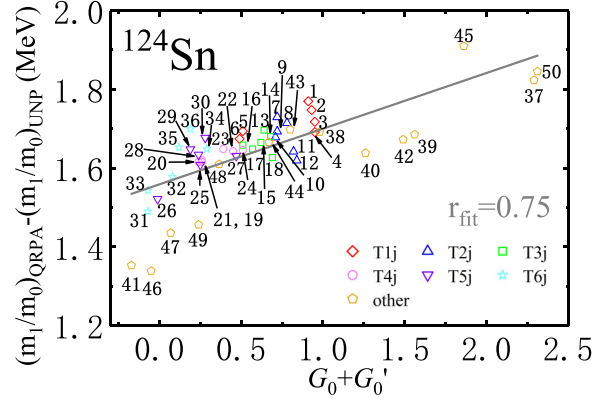
strength W_0, i.e., the larger the value of α the smaller the spin-orbit splitting is.

C. QRPA correlations and tensor terms

We now study how the QRPA energies correlate with the tensor terms and also with the main part of the QRPA residual interactions, which are associated with the Landau parameters G_0 and G_0'. Figures 6(a) and 6(b) shows the correlations between the low-lying and high-lying $M1$ states and the tensor terms α and β, respectively. In panel (a), the low-lying $M1$ peaks show a clear anticorrelation with the value of α, which can be understood because of a smaller spin-orbit splitting caused by a larger α value, as discussed in the previous subsection. On the other hand, the correlation is rather weak for the high-lying states. It might be due to the strong QRPA correlations for the high-lying states as will be discussed below. In the right panel, the correlations between the $M1$ energies and β value is very modest, showing a small anticorrelation effect.

In Fig. 7, we study the correlation between the sum of the Landau parameters $G_0 + G_0'$ and the difference of centroid energies of QRPA and unperturbed strengths, where the centroid

FIG. 6. The QRPA energies of low-lying and high-lying $M1$ peaks for ^{124}Sn as a function of α for each fixed β (figure (a)), and as a function of β for each fixed α (b). The theoretical values are calculated by using the Tij parameter sets with tensor force.

energy is defined by the ratio of the energy-weighted sum rule m_1 to the non-energy-weighted sum rule m_0. $(m_1/m_0)_{\text{QRPA}}$ and $(m_1/m_0)_{\text{UNP}}$ in the figure are the calculated centroid energies of QRPA and unperturbed strengths, respectively. We can see a clear linear correlation between the sum of Landau parameters and the centroid energies. This correlation can be understood within a simple two levels model in the following.

In the QRPA response, there are two main unperturbed configurations in ^{124}Sn: the proton configuration $1g_{9/2} \rightarrow 1g_{7/2}$ and the neutron one $1h_{11/2} \rightarrow 1h_{9/2}$, as already mentioned in the previous subsection. The energy of the proton (neutron) two-quasiparticle configuration can be represented as $\varepsilon_p(\varepsilon_n)$. The QRPA matrix is, then, schematically expressed as

$$\begin{pmatrix} \varepsilon_p + v_0 & v_1 \\ v_1 & \varepsilon_n + v_0 \end{pmatrix},$$

where $v_0 = G_0 + G_0'$ is the pp or nn interaction while $v_1 = G_0 - G_0'$ is the pn interaction. We remind that G_0 and G_0' represent the Landau parameters in the spin channel $\vec{\sigma}_1 \cdot \vec{\sigma}_2$ and spin-isospin channel $(\vec{\sigma}_1 \cdot \vec{\sigma}_2)(\vec{\tau}_1 \cdot \vec{\tau}_2)$, respectively. If we diagonalize the matrix, the two eigenvalues can be written as

$$\hbar\omega_1 = \frac{\varepsilon_p + \varepsilon_n}{2} + v_0 - \frac{\sqrt{(\varepsilon_p + \varepsilon_n)^2 + 4v_1^2}}{2},$$

$$\hbar\omega_2 = \frac{\varepsilon_p + \varepsilon_n}{2} + v_0 + \frac{\sqrt{(\varepsilon_p + \varepsilon_n)^2 + 4v_1^2}}{2}.$$

On the other hand, according to the definition of the centroid energy

$$\left(\frac{m_1}{m_0}\right)_{\text{QRPA}} = \frac{1}{2}(\hbar\omega_1 + \hbar\omega_2),$$

$$\left(\frac{m_1}{m_0}\right)_{\text{UNP}} = \frac{1}{2}(\varepsilon_p + \varepsilon_n).$$

Therefore, there is a correlation expressed by

$$\left(\frac{m_1}{m_0}\right)_{\text{QRPA}} - \left(\frac{m_1}{m_0}\right)_{\text{UNP}} = G_0 + G_0'.$$

This positive correlation is clearly demonstrated in Fig. 7.

We will now compare the calculated $M1$ strength distributions of ^{124}Sn with the experimental data obtained by (p, p') scattering in Ref. [32]. The QRPA strength distributions of ^{124}Sn calculated by using several Tij and other Skyrme EDFs are shown in Fig. 2. In Fig. 2(a)–2(d), the Tij EDFs are employed: (a) changing α for a fixed value $\beta = -60$ MeV fm^5; (b) changing β for a fixed value $\alpha = -60$ MeV fm^5; (c) in the case $\alpha = \beta = (-60, 60, 180)$ MeV fm^5, corresponding to $i = j = (1, 3, 5)$; (d) in the cases $\alpha \neq \beta$ that are not shown in (a)–(c), including T24, T42, T35, T53, T46, and T64, except T11. Figures 2(e) and 2(f) correspond instead to the case of commonly used Skyrme EDFs without the tensor terms, except SLy5 which has the tensor terms.

As expected from Fig. 6(a), the peak position of the $M1$ strength becomes lower for larger α. The same trend can be seen also in Fig. 6(b) when varying the value of β, while the change of peak energy is rather modest. One can find the same

TABLE I. Parameters of the tensor terms and J terms in units of MeV fm^5.

	T	U	α	β	α_C	β_C	α_T	β_T
SLy5	888.0	−408.0	−89.8	51.1	80.2	−48.9	−170.0	100.0
T11	258.9	−342.8	−60.0	−60.0	82.8	−42.5	−142.8	−17.5
T15	−500.9	173.3	180.0	−60.0	107.8	8.3	72.2	−68.3

trend also in Figs. 2(a) and 2(b), i.e., the larger tensor terms give lower peak energies. In Figs. 2(e) and 2(f), the results depend on both the Landau parameters and the spin-orbit coupling W_0.

Eventually, from Fig. 2, it is found that the sets T11 and SLy5 with tensor force give better description of the strength distribution in ^{124}Sn compared to the other parameter sets, in terms of the peak height and the peak position. Because of this reason, in the following, the T11 and SLy5 Skyrme EDFs with and without tensor terms [36,40,69] will be studied in more detail. Table I displays the values of T, U, α, β, α_C, β_C, α_T, and β_T in Eqs. (7), (9), and (10) for the Skyrme parameter sets T11 and SLy5. It is found that the values of α of the two parameter sets are negative. α can be positive in some Tij sets, by definition, from Eq. (12). As a counter example to T11 and SLy5, the T15 parameter set is also chosen in the following calculations for $M1$ states.

D. $M1$ of $^{112-120,124}$Sn

As discussed in the Introduction, the RPA or QRPA with Skyrme interactions has been used for many years in the description of $M1$ resonance in finite nuclei. Previously, we have systematically studied the effect of tensor terms on the magnetic dipole resonances in ^{48}Ca and ^{208}Pb with various Skyrme interactions [45,46]. Recently, the strength distributions of magnetic dipole resonances in even-even $^{112-120,124}$Sn isotopes have been measured at RCNP [31,32]. This work extends our study to the magnetic dipole resonances in Sn isotopes using the QRPA approach with the SLy5 and T11 parameter sets. In Figs. 8 and 9, the $M1$ strength distributions of $^{112-120,124}$Sn are shown, respectively. The results with and without tensor interaction are both compared with the available experimental data [31,32].

From the figures, basically, one can find that the calculated response functions with and without tensor force in $^{112-120}$Sn both display three resonance peaks, namely, the low-lying $M1$ pygmy state, the $M1$ main peak, and the one appearing at higher energy. The three states are mainly formed by the neutron $\nu 2d_{5/2} \rightarrow \nu 2d_{3/2}$, proton $\pi 1g_{9/2} \rightarrow \pi 1g_{7/2}$, and neutron $\nu 1h_{11/2} \rightarrow \nu 1h_{9/2}$ configurations, respectively. For $^{112-116}$Sn, $M1$ main peaks with a shoulder are found. The state that forms the shoulder comes from the neutron $\nu 1g_{9/2} \rightarrow \nu 1g_{7/2}$ configuration, and its strength is reduced and disappears in ^{118}Sn because the occupation probability of neutron state $\nu 1g_{7/2}$ is becoming larger and the transition probability of neutron $\nu 1g_{9/2} \rightarrow \nu 1g_{7/2}$ configuration is becoming smaller with increasing mass number. The magnetic dipole strength distribution of ^{124}Sn displays the strong $M1$ peak arising from the proton $\pi 1g_{9/2} \rightarrow \pi 1g_{7/2}$ configuration and the
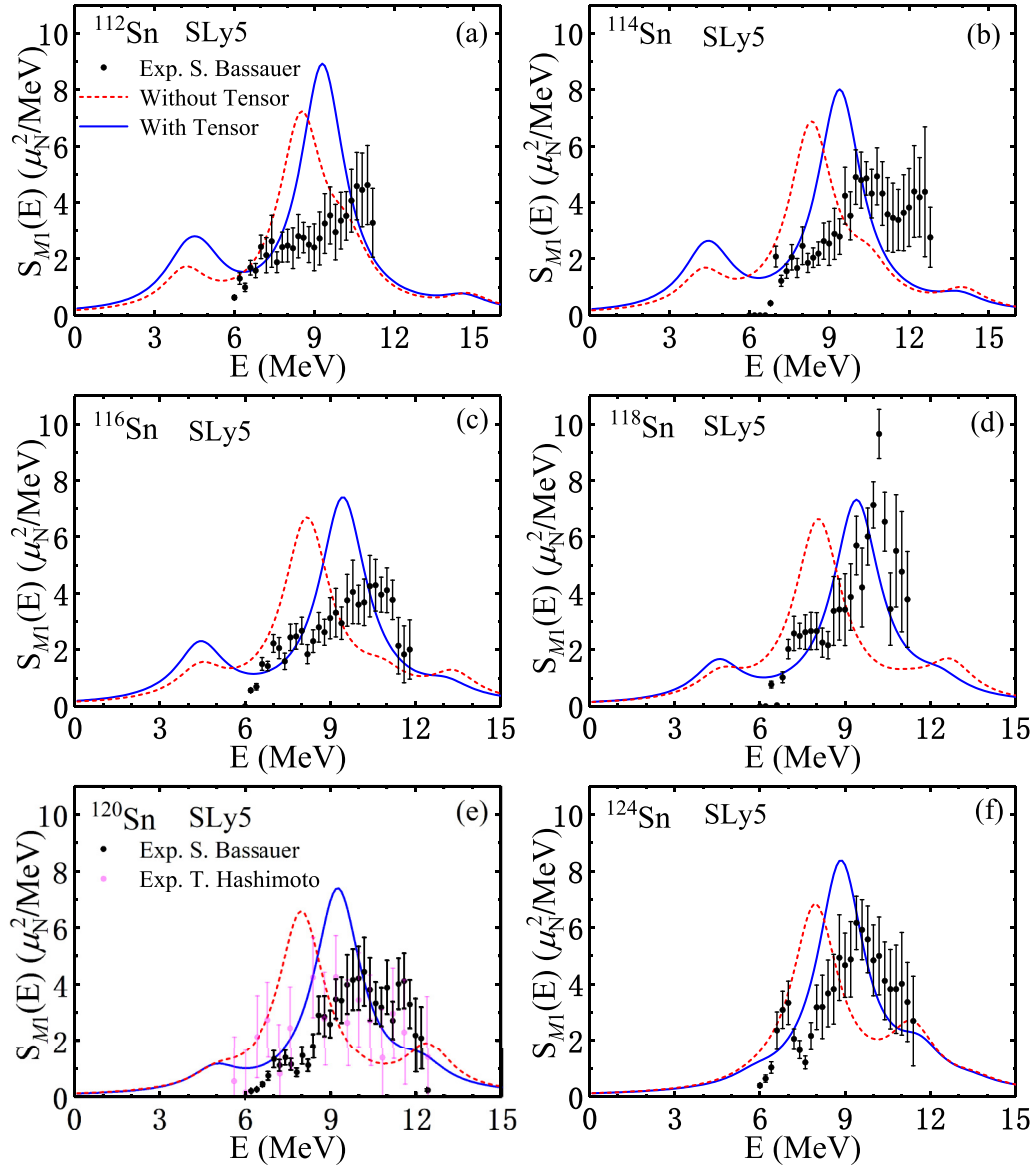
FIG. 8. The QRPA strength distributions of $^{112-120,124}$Sn, calculated by using the SLy5 Skyrme interaction. The results with and without tensor terms are both shown, and compared with the experimental data [31,32]. Calculated strengths are convoluted by a Lorentzian shape with a width of 2.0 MeV.

higher energy state based on the neutron $\nu 1h_{11/2} \rightarrow \nu 1h_{9/2}$ configuration, while the pygmy state in the low energy region is not evident.

As for the experimental results shown in the figures, the current researches [31,32] on $^{112-120,124}$Sn have only provided the magnetic dipole strength distributions between 6.0 MeV and 12.0 MeV for all studied nuclei. Our calculations reveal some pygmy strengths emerging below 6.0 MeV in $^{112-120}$Sn, which mainly arise from the neutron configuration $\nu 2d_{5/2} \rightarrow \nu 2d_{3/2}$. It is seen that the strengths of these pygmy states become weaker with increasing mass number. This is because the occupation probabilities of neutron states $\nu 2d_{3/2}$ in these nuclei are becoming larger, and the transition probabilities between $\nu 2d_{5/2}$ and $\nu 2d_{3/2}$ are reduced along the Sn isotopes. As expected, the positions of the predicted pygmy peaks depend on the energy splittings of the two spin-orbit partners. In the

Skyrme HF-BCS calculation, the spin-orbit potential $U_{s.o.}$ has the dominant contributions from the spin-orbit strength W_0 as well as the spin-orbit densities J weighted by the tensor parameters α_T and β_T, as shown in Eqs. (7) and (10). SLy5 and T11 interactions with tensor terms had been successfully applied to predict the spin-orbit splittings of finite nuclei. For example, in Refs. [36,81], it is shown that SLy5 interaction with tensor terms can fairly well explain the isospin dependence of energy differences $\varepsilon(\pi\,1h_{11/2}) - \varepsilon(\pi\,1g_{7/2})$ along Sn isotopes, and $\varepsilon(\nu\,1i_{13/2}) - \varepsilon(\nu\,1h_{9/2})$ along $N = 82$ isotones, as well as $\varepsilon(\pi\,2s_{1/2}) - \varepsilon(\pi\,1d_{3/2})$ along Ca isotopes. Furthermore, the $1f$ spin-orbit splittings in ^{40,48}Ca calculated by T11 show reasonable agreement with the measurements as mentioned in Ref. [82]. From these good features of the spin-orbit splittings, we expect that SLy5 and T11 EDFs with tensor terms can give reasonable predictions of the spin-orbit
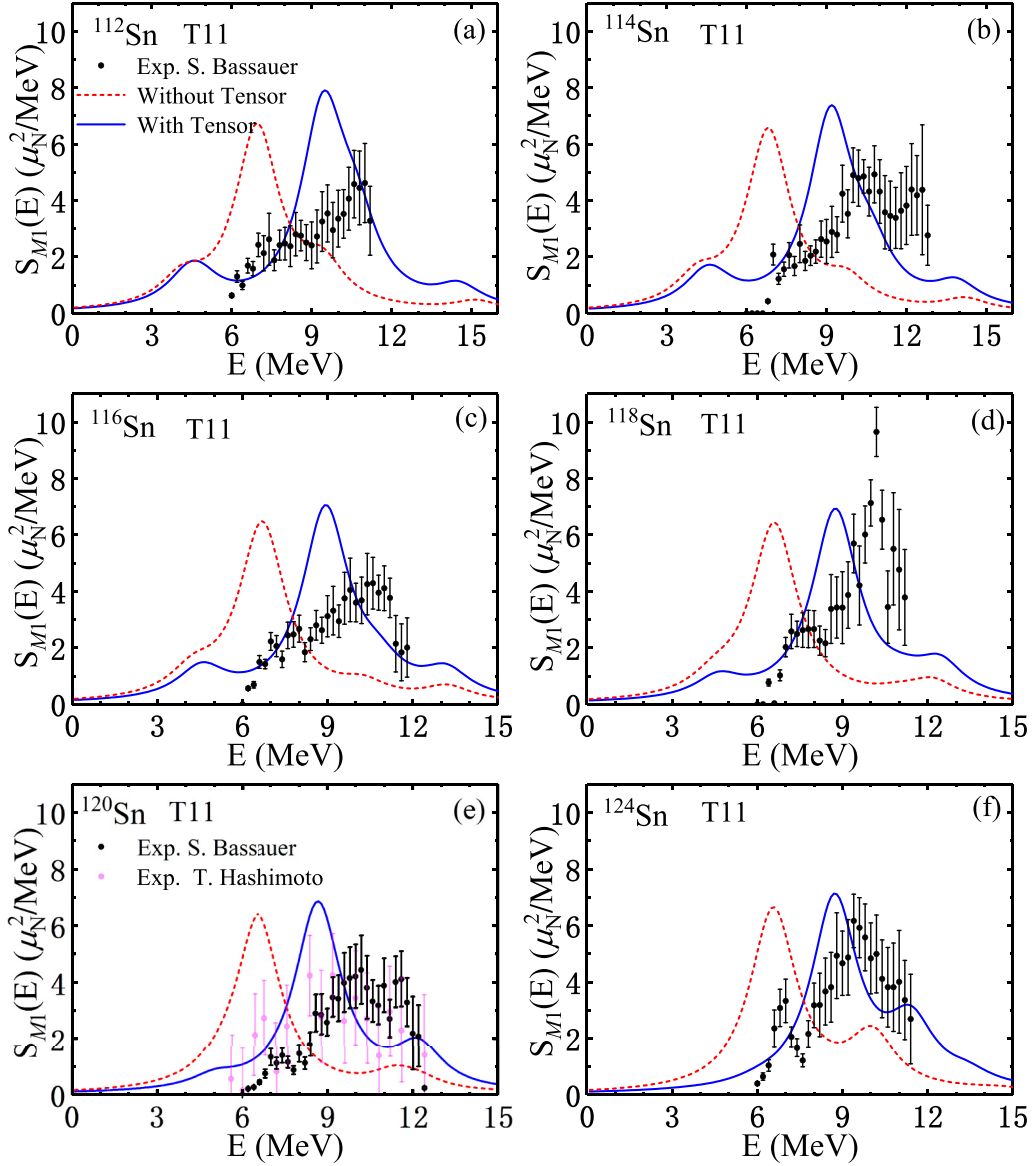
FIG. 9. The same as Fig. 8, but calculated with T11.

splittings of neutron states $2d_{5/2}$ and $2d_{3/2}$ in Sn isotopes. It would be quite interesting if these pygmy distributions could be further confirmed by the experiments in the future.

E. Effect of tensor force on $M1$ of ^{112}Sn and ^{124}Sn

Although the experimental results have large error bars at high energy, and in a few cases (the lighter $^{112-114}$Sn isotopes) the main peaks do not emerge clearly, still it is clear from Figs. 8 and 9 that the results calculated by SLy5 and T11 with tensor can give a better description of the experimental strength distributions of $^{112-120,124}$Sn as compared to the results without the tensor force. To understand how the tensor force changes the strength distribution, we will take ^{112}Sn and ^{124}Sn as an example to show the mechanism. The effects of tensor force on the Hartree-Fock and QRPA peaks have been discussed in Refs. [45,46], and we will follow the same method in present analysis. The effect of tensor force on

QRPA states can be estimated by the following formula where ΔE_{QRPA} represents the difference between the QRPA results with and without tensor force

$$\Delta E_{\mathrm{QRPA}} \approx \Delta E_{\mathrm{HF}} + \langle V_{\mathrm{tensor}} \rangle. \tag{13}$$

The first term in the right describes the change in the HF peak(s), and the second term is the average of the effect from the residual tensor interaction in QRPA calculation. The calculated Hartree-Fock and QRPA $M1$ strength distributions of ^{112}Sn and ^{124}Sn obtained by using the SLy5 and T11 parameter sets with and without tensor force are shown in Figs. 10 and 11, respectively. The corresponding numerical data are shown in detail in Tables II and III. For the Hartree-Fock strengths of ^{112}Sn shown in Fig. 10(a), the results are obtained using the SLy5 interaction with and without tensor force. The unperturbed state associated with the configuration $\pi 1g_{9/2} \rightarrow \pi 1g_{7/2}$ is pushed upward from 6.57 MeV to 8.18 MeV when the tensor force is included in the calculation.

FIG. 10. The $M1$ Hartree-Fock and QRPA strength distributions of ^{112}Sn obtained using the SLy5 and T11 parameter sets in the cases with and without tensor force.
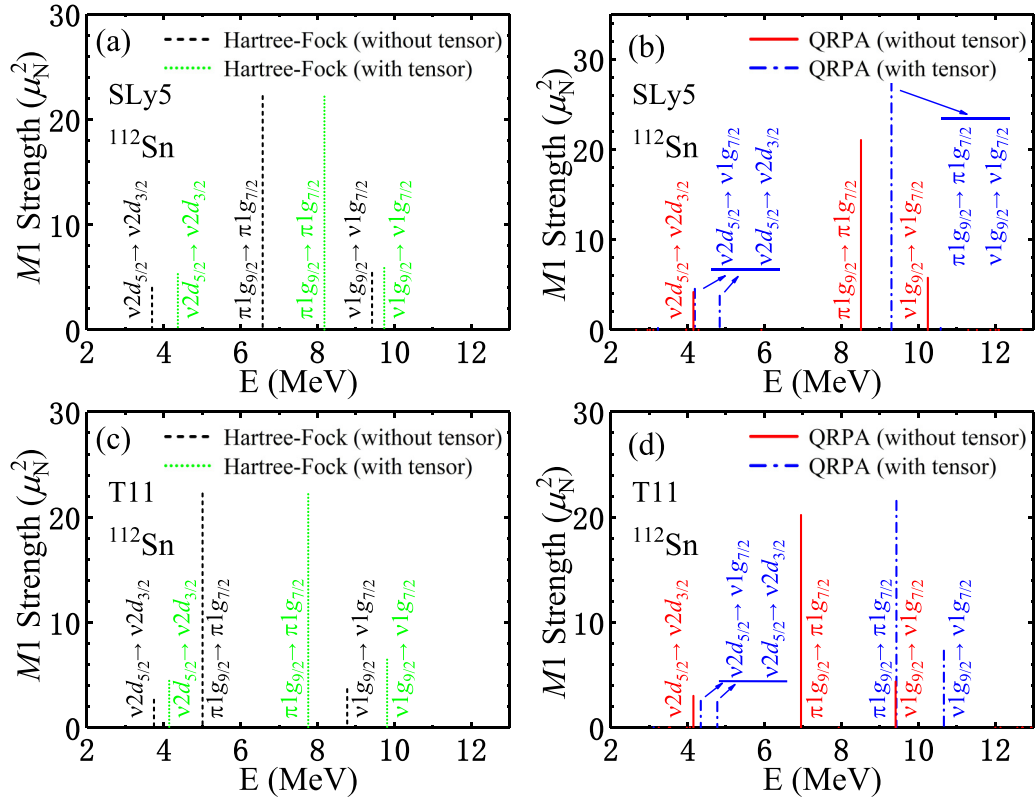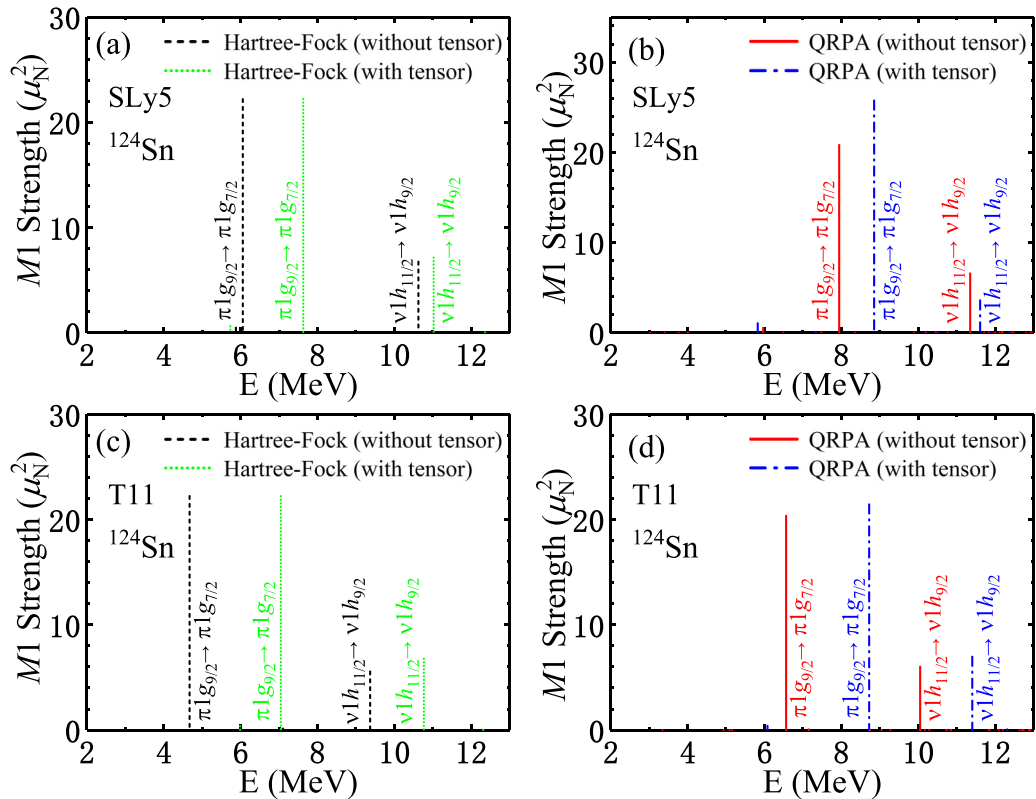

FIG. 11. The $M1$ Hartree-Fock and QRPA strength distributions of ^{124}Sn obtained using theSLy5 and T11 parameter sets in the cases with and without tensor force.

TABLE II. The Hartree-Fock and QRPA energies, the two-quasiparticle configurations which give the main contribution to the excited state, and $X_\nu^2 - Y_\nu^2$ (only for QRPA state). The results are calculated for ^{112}Sn with SLy5 and T11 interactions with and without tensor force.

| | without tensor | | | | | with tensor | | | | |
| | Hartree-Fock | | QRPA | | | Hartree-Fock | | QRPA | | |
force SLy5	E_ν	config.	E_ν	config.	X_ν^2-Y_ν^2	E_ν	config.	E_ν	config.	X_ν^2-Y_ν^2
	3.70	$\left(2d_{\frac{5}{2}}2d_{\frac{3}{2}}^{-1}\right)^\nu$	4.15	$\left(2d_{\frac{5}{2}}2d_{\frac{3}{2}}^{-1}\right)^\nu$	99.1	4.37	$\left(2d_{\frac{5}{2}}2d_{\frac{3}{2}}^{-1}\right)^\nu$	4.19	$\left(2d_{\frac{5}{2}}1g_{\frac{7}{2}}^{-1}\right)^\nu$	62.0
									$\left(2d_{\frac{5}{2}}2d_{\frac{3}{2}}^{-1}\right)^\nu$	36.2
	6.57	$\left(1g_{\frac{9}{2}}1g_{\frac{7}{2}}^{-1}\right)^\pi$	8.51	$\left(1g_{\frac{9}{2}}1g_{\frac{7}{2}}^{-1}\right)^\pi$	99.5	8.18	$\left(1g_{\frac{9}{2}}1g_{\frac{7}{2}}^{-1}\right)^\pi$	4.84	$\left(2d_{\frac{5}{2}}1g_{\frac{7}{2}}^{-1}\right)^\nu$	37.2
									$\left(2d_{\frac{5}{2}}2d_{\frac{3}{2}}^{-1}\right)^\nu$	59.8
	9.42	$\left(1g_{\frac{9}{2}}1g_{\frac{7}{2}}^{-1}\right)^\nu$	10.25	$\left(1g_{\frac{9}{2}}1g_{\frac{7}{2}}^{-1}\right)^\nu$	99.0	9.74	$\left(1g_{\frac{9}{2}}1g_{\frac{7}{2}}^{-1}\right)^\nu$	9.31	$\left(1g_{\frac{9}{2}}1g_{\frac{7}{2}}^{-1}\right)^\pi$	78.4
									$\left(1g_{\frac{9}{2}}1g_{\frac{7}{2}}^{-1}\right)^\nu$	15.7
T11	E_ν	config.	E_ν	config.	X_ν^2-Y_ν^2	E_ν	config.	E_ν	config.	X_ν^2-Y_ν^2
	3.75	$\left(2d_{\frac{5}{2}}2d_{\frac{3}{2}}^{-1}\right)^\nu$	4.15	$\left(2d_{\frac{5}{2}}2d_{\frac{3}{2}}^{-1}\right)^\nu$	98.8	4.14	$\left(2d_{\frac{5}{2}}2d_{\frac{3}{2}}^{-1}\right)^\nu$	4.34	$\left(2d_{\frac{5}{2}}1g_{\frac{7}{2}}^{-1}\right)^\nu$	53.4
									$\left(2d_{\frac{5}{2}}2d_{\frac{3}{2}}^{-1}\right)^\nu$	46.2
	5.01	$\left(1g_{\frac{9}{2}}1g_{\frac{7}{2}}^{-1}\right)^\pi$	6.95	$\left(1g_{\frac{9}{2}}1g_{\frac{7}{2}}^{-1}\right)^\pi$	99.6	7.76	$\left(1g_{\frac{9}{2}}1g_{\frac{7}{2}}^{-1}\right)^\pi$	4.78	$\left(2d_{\frac{5}{2}}1g_{\frac{7}{2}}^{-1}\right)^\nu$	46.3
									$\left(2d_{\frac{5}{2}}2d_{\frac{3}{2}}^{-1}\right)^\nu$	52.0
	8.78	$\left(1g_{\frac{9}{2}}1g_{\frac{7}{2}}^{-1}\right)^\nu$	9.41	$\left(1g_{\frac{9}{2}}1g_{\frac{7}{2}}^{-1}\right)^\nu$	99.5	9.81	$\left(1g_{\frac{9}{2}}1g_{\frac{7}{2}}^{-1}\right)^\nu$	9.43	$\left(1g_{\frac{9}{2}}1g_{\frac{7}{2}}^{-1}\right)^\pi$	96.6
									10.67	$\left(1g_{\frac{9}{2}}1g_{\frac{7}{2}}^{-1}\right)^\nu$	97.2

Similarly, the tensor force moves the low-lying state related to $\nu2d_{5/2} \to \nu2d_{3/2}$ configuration from 3.70 MeV to 4.37 MeV. For the higher energy state arising from $\nu1g_{9/2} \to \nu1g_{7/2}$ configuration, its energy is slightly shifted upward from 9.42 MeV to 9.74 MeV. This means that the spin-orbit splittings of partner levels are enlarged when the tensor force is involved, with this choice of parameters. In fact, it should be noticed by looking at Eq. (7) that the negative value of $U(\alpha_T)$ is essential to enlarge the spin-orbit splitting, and produces a better agreement with the experimental data as a net result.

The effect of tensor force on the QRPA strengths based on SLy5 interaction is shown in Fig. 10(b). Without including the tensor interaction, the main $M1$ resonance state coming from the proton configuration $1g_{9/2} \to 1g_{7/2}$ lies at 8.51 MeV, and the low-lying state formed from the neutron configuration $2d_{5/2} \to 2d_{3/2}$ appears at 4.15 MeV. When the tensor force is taken into account, the $M1$ main resonance peak is pushed up to 9.31 MeV, being this peak mainly composed of the proton $\pi1g_{9/2} \to \pi1g_{7/2}$ configuration with an admixture of the neutron $\nu1g_{9/2} \to \nu1g_{7/2}$ configuration. As for the low-lying QRPA states, there are two states located at energies

TABLE III. The Hartree-Fock and QRPA energies, the two-quasiparticle configurations which gives the main contribution to the excited state, and $X_\nu^2 - Y_\nu^2$ (only for QRPA state). The results are calculated for ^{124}Sn with SLy5 and T11 interactions with and without tensor force.

| | without tensor | | | | | with tensor | | | | |
| | Hartree-Fock | | QRPA | | | Hartree-Fock | | QRPA | | |
force SLy5	E_ν	config.	E_ν	config.	X_ν^2-Y_ν^2	E_ν	config.	E_ν	config.	X_ν^2-Y_ν^2
	6.06	$\left(1g_{\frac{9}{2}}1g_{\frac{7}{2}}^{-1}\right)^\pi$	7.95	$\left(1g_{\frac{9}{2}}1g_{\frac{7}{2}}^{-1}\right)^\pi$	99.5	7.63	$\left(1g_{\frac{9}{2}}1g_{\frac{7}{2}}^{-1}\right)^\pi$	8.85	$\left(1g_{\frac{9}{2}}1g_{\frac{7}{2}}^{-1}\right)^\pi$	92.2
	10.63	$\left(1h_{\frac{11}{2}}1h_{\frac{9}{2}}^{-1}\right)^\nu$	11.35	$\left(1h_{\frac{11}{2}}1h_{\frac{9}{2}}^{-1}\right)^\nu$	97.9	11.02	$\left(1h_{\frac{11}{2}}1h_{\frac{9}{2}}^{-1}\right)^\nu$	11.61	$\left(1h_{\frac{11}{2}}1h_{\frac{9}{2}}^{-1}\right)^\nu$	92.2
T11	E_ν	config.	E_ν	config.	X_ν^2-Y_ν^2	E_ν	config.	E_ν	config.	X_ν^2-Y_ν^2
	4.68	$\left(1g_{\frac{9}{2}}1g_{\frac{7}{2}}^{-1}\right)^\pi$	6.56	$\left(1g_{\frac{9}{2}}1g_{\frac{7}{2}}^{-1}\right)^\pi$	99.7	7.05	$\left(1g_{\frac{9}{2}}1g_{\frac{7}{2}}^{-1}\right)^\pi$	8.72	$\left(1g_{\frac{9}{2}}1g_{\frac{7}{2}}^{-1}\right)^\pi$	96.8
	9.37	$\left(1h_{\frac{11}{2}}1h_{\frac{9}{2}}^{-1}\right)^\nu$	10.05	$\left(1h_{\frac{11}{2}}1h_{\frac{9}{2}}^{-1}\right)^\nu$	99.3	10.77	$\left(1h_{\frac{11}{2}}1h_{\frac{9}{2}}^{-1}\right)^\nu$	11.41	$\left(1h_{\frac{11}{2}}1h_{\frac{9}{2}}^{-1}\right)^\nu$	96.1

4.19 MeV and 4.84 MeV, which are formed by the neutron configurations $2d_{5/2} \rightarrow 1g_{7/2}$ and $2d_{5/2} \rightarrow 2d_{3/2}$, where each configuration gives different contribution to the QRPA states as shown in Table II.

From Table II, one can extract that ΔE_{QRPA} is 0.80 MeV and ΔE_{HF} equals to 1.61 MeV for the $M1$ main peak of ^{112}Sn with the SLy5 interaction. Therefore, this leads to $\langle V_{\text{tensor}} \rangle = -0.81$ MeV. Since the low-lying state is separated into two states when the tensor force is included, we use the average value as the QRPA result, that is, 4.52 MeV. ΔE_{QRPA} is about 0.37 MeV and ΔE_{HF} is equal to 0.67 MeV for the low-lying state, so that the value of $\langle V_{\text{tensor}} \rangle$ is extracted to be -0.30 MeV. The extracted values of $\langle V_{\text{tensor}} \rangle$ disclose that the tensor force is attractive. This is consistent with the conclusion in Ref. [45].

For the results of ^{112}Sn with the T11 interaction, both the Hartree-Fock and QRPA strengths are pushed upward when the tensor force is included in the calculations, as shown in Fig. 10(c) and 10(d). From Table II, one can obtain that the unperturbed states associated with the $\nu 2d_{5/2} \rightarrow \nu 2d_{3/2}$, $\pi 1g_{9/2} \rightarrow \pi 1g_{7/2}$, and $\nu 1g_{9/2} \rightarrow \nu 1g_{7/2}$ configurations move upward by 0.39, 2.75, and 1.03 MeV, respectively, as an effect of the tensor force. In the QRPA strengths, the energy changes of the low-lying, main $M1$, and higher energy states are 0.41, 2.48, and 1.26 MeV with the tensor force, respectively. Using Eq. (13), we can extract that $\langle V_{\text{tensor}} \rangle = 0.02, -0.27$, and 0.23 MeV, respectively. One can see that, in comparison with the results of SLy5 interaction, the residual tensor force of T11 interaction shows attraction for main peak but repulsion for the low-lying and high-lying states.

We now analyze the results of ^{124}Sn obtained using SLy5 and T11, with and without tensor force. At variance with the case of ^{112}Sn, there are only two Hartree-Fock or QRPA states shown in Fig. 11 and Table III: one low-lying and one high-lying state, which are formed mainly from the proton $\pi 1g_{9/2} \rightarrow \pi 1g_{7/2}$ configuration and neutron $\nu 1h_{11/2} \rightarrow \nu 1h_{9/2}$ configuration, respectively. In the unperturbed strength obtained by SLy5 without the tensor force in Fig. 11(a), the low-lying unperturbed state lies at 6.06 MeV, while the high-lying state is at 10.63 MeV. As mentioned previously, when the tensor force is included, the spin-orbit splittings are enlarged, and the corresponding states are pushed upward to 7.63 and 11.02 MeV, respectively. For the QRPA states without the tensor force in Fig. 11(b), one can find that the low-lying state is located at 7.95 MeV while the high energy state is at 11.35 MeV, and they are pushed upward to 8.85 and 11.61 MeV by the tensor, respectively. According to Eq. (13) and Table III, the extracted values of $\langle V_{\text{tensor}} \rangle$ for low-lying and high-lying states are -0.67 and -0.13 MeV, respectively. These results also reveal that the residual tensor force associated with the SLy5 set provides attractive contributions. In the case of the T11 interaction, the results obtained with and without tensor force are shown in Fig. 11(c) and 11(d) and Table III. Because the tensor force enlarges the spin-orbit splittings also in the case of the T11 interaction, the calculated ΔE_{HF} of the unperturbed low-lying and high-lying states are 2.37 and 1.40 MeV, respectively. For the QRPA strengths, the values of ΔE_{QRPA} for the two states are about 2.16 and 1.36 MeV. So, the contributions of the residual tensor force in

Eq. (13) for the low-lying and high-lying states are extracted to be -0.21 and -0.04 MeV. Similar to the situation in ^{112}Sn, the residual tensor force of T11 interaction for ^{124}Sn shows weak attraction in the QRPA calculation.

In summary, SLy5 and T11 interactions with tensor force provide reasonable description of the experimental magnetic dipole data in $^{112-120,124}$Sn in comparisons with other Tij members and also the cases without tensor force. In other terms, we have checked that other forces, like those without tensor terms and the other Tij sets, are less good when compared with experimental data. This is shown in Fig. 2 (cf. also the discussion). By looking at Table I, one can easily see that these results strongly suggest negative values of α, whereas no clear constraint emerges for β. We remind that α is associated with the tensor interaction between like-particle, while β is associated with the tensor interaction between protons and neutrons.

There are indeed other parameter sets with positive α_T, like the T15 interaction shown in Table I, which give an opposite effect on the $M1$ resonance. We take ^{112}Sn and ^{124}Sn as an example to explore the role of tensor force with the T15 interaction. Figures 12(a) and 12(b) show the Hartree-Fock and QRPA strength distributions of ^{112}Sn, while Fig. 12(c) and 12(d) do the same for the Hartree-Fock and QRPA strength distributions of ^{124}Sn. As shown in Fig. 12(a), the $M1$ main peak in ^{112}Sn coming from the proton configuration $\pi 1g_{9/2} \rightarrow \pi 1g_{7/2}$ has a clear downward shift, $\Delta E_{\text{HF}} = -0.43$ MeV, with the tensor interaction. This could be understood as follows: in the proton states in the $Z = 50$ core, only the $1g_{9/2}$ orbital gives positive contribution to the spin density $J_p > 0$ [36]. On the other hand, the neutron states $1g_{9/2}$, $2d_{5/2}$, $1g_{7/2}$, $2d_{3/2}$, $3s_{1/2}$, and $1h_{11/2}$ are partially occupied, and the neutron spin density J_n is positive but smaller than J_p. According to Eqs. (7) and (10), and together with the values of α_T and β_T of T15 (shown in Table I), the tensor force provides a positive contribution to the proton spin $-$ orbit potential $U_{\text{s.o.}}^{(p)}$, which makes $U_{\text{s.o.}}^{(p)}$ weaker. As a result, the spin-orbit splittings of proton states are reduced, so one gets negative ΔE_{HF}. This leads to the downward shift of the main peak. In the QRPA case, based on Eq. (13) and Table IV, we can extract that ΔE_{QRPA} is about -0.98 MeV, so the contribution of the residual tensor force $\langle V_{\text{tensor}} \rangle$ is equal to -0.55 MeV. A similar pattern is also seen in the case of ^{124}Sn with the T15 interaction. The shift of the $M1$ main state in the Hartree-Fock response is -0.41 MeV, while ΔE_{QRPA} and $\langle V_{\text{tensor}} \rangle$ are -0.96 and -0.55 MeV, respectively.

F. Quenching factor

Finally, we will discuss the quenching problem for $M1$ resonances. Table V shows the experimental total transition strengths [32], the calculated total QRPA transition strengths and corresponding quenching factors for $^{112-120,124}$Sn isotopes. The results are calculated by using the Skyrme interactions SLy5 and T11 with and without tensor force. The values in the parentheses are obtained in the case of without tensor force. On the one hand, as shown in Table V, the calculated total QRPA transition strengths $\sum B_{M1}^{\text{th}}$ with and without tensor both overestimate the experimental data. On
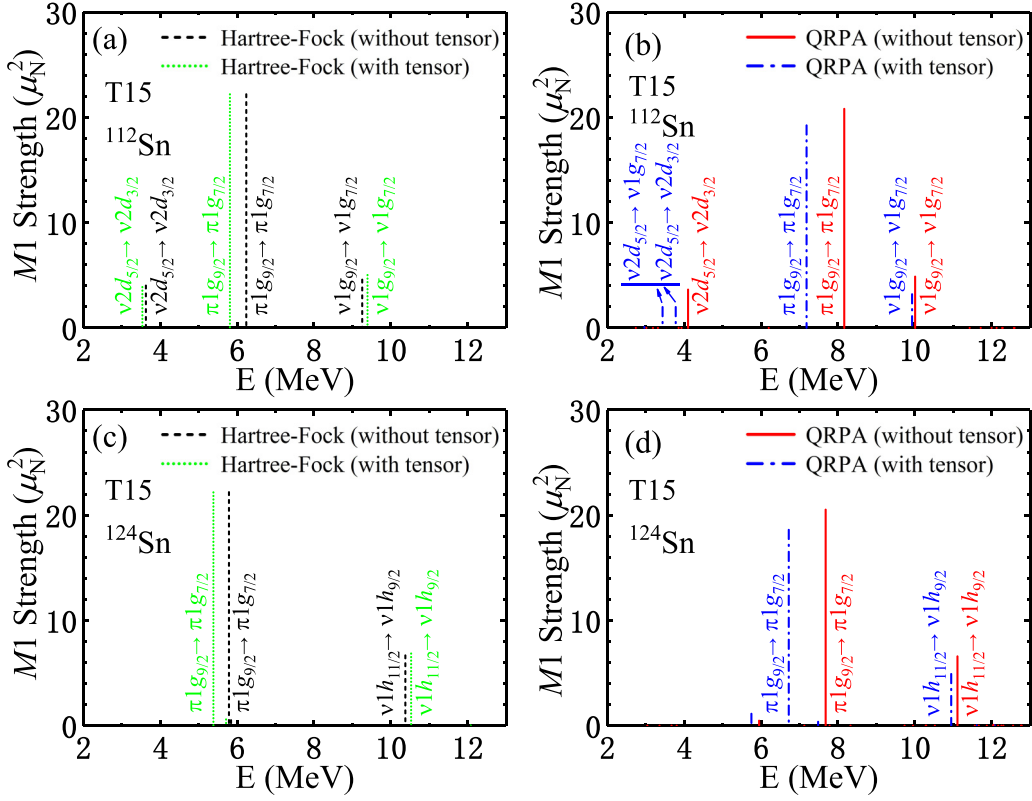
FIG. 12. The $M1$ Hartree-Fock and QRPA strength distributions of ^{112}Sn and ^{124}Sn obtained using the T15 parameter set in the cases with and without tensor force.

the other hand, although the SLy5 and T11 interactions with tensor force can describe well the strength distributions of $M1$ resonances for all nuclei, the summed transition probabilities obtained by SLy5 and T11 interactions deviate from the experimental data even when the tensor terms are included.

The total $M1$ transition strengths predicted by QRPA are in general larger than experimental data when the free values of the g factors are used. Therefore the free values are often modified by taking implicity into account many-body effects, mesonic currents, and Δ-hole excitations, to obtain better

TABLE IV. The Hartree-Fock and QRPA energies, the two-quasiparticle configurations which gives the main contribution to the excited state, and $X_\nu^2 - Y_\nu^2$ (only for QRPA state). The results are calculated for ^{112}Sn and ^{124}Sn with T15 interaction with and without tensor force.

| | without tensor | | | | with tensor | | | |
| | Hartree-Fock | | QRPA | | | Hartree-Fock | | QRPA | |
^{112}Sn	E_ν	config.	E_ν	config.	X_ν^2-Y_ν^2	E_ν	config.	E_ν	config.	X_ν^2-Y_ν^2
	3.63	$\left(2d_{\frac{5}{2}}2d_{\frac{3}{2}}^{-1}\right)^\nu$	4.10	$\left(2d_{\frac{5}{2}}2d_{\frac{3}{2}}^{-1}\right)^\nu$	99.3	3.54	$\left(2d_{\frac{5}{2}}2d_{\frac{3}{2}}^{-1}\right)^\nu$	3.44	$\left(2d_{\frac{5}{2}}1g_{\frac{7}{2}}^{-1}\right)^\nu$	68.6
									$\left(2d_{\frac{5}{2}}2d_{\frac{3}{2}}^{-1}\right)^\nu$	29.7
	6.24	$\left(1g_{\frac{9}{2}}1g_{\frac{7}{2}}^{-1}\right)^\pi$	8.17	$\left(1g_{\frac{9}{2}}1g_{\frac{7}{2}}^{-1}\right)^\pi$	99.7	5.81	$\left(1g_{\frac{9}{2}}1g_{\frac{7}{2}}^{-1}\right)^\pi$	3.78	$\left(2d_{\frac{5}{2}}1g_{\frac{7}{2}}^{-1}\right)^\nu$	30.3
									$\left(2d_{\frac{5}{2}}2d_{\frac{3}{2}}^{-1}\right)^\nu$	67.0
	9.25	$\left(1g_{\frac{9}{2}}1g_{\frac{7}{2}}^{-1}\right)^\nu$	10.01	$\left(1g_{\frac{9}{2}}1g_{\frac{7}{2}}^{-1}\right)^\nu$	99.1	9.39	$\left(1g_{\frac{9}{2}}1g_{\frac{7}{2}}^{-1}\right)^\nu$	7.19	$\left(1g_{\frac{9}{2}}1g_{\frac{7}{2}}^{-1}\right)^\pi$	97.9
								9.93	$\left(1g_{\frac{9}{2}}1g_{\frac{7}{2}}^{-1}\right)^\nu$	98.5
^{124}Sn	E_ν	config.	E_ν	config.	X_ν^2-Y_ν^2	E_ν	config.	E_ν	config.	X_ν^2-Y_ν^2
	5.79	$\left(1g_{\frac{9}{2}}1g_{\frac{7}{2}}^{-1}\right)^\pi$	7.68	$\left(1g_{\frac{9}{2}}1g_{\frac{7}{2}}^{-1}\right)^\pi$	99.7	5.38	$\left(1g_{\frac{9}{2}}1g_{\frac{7}{2}}^{-1}\right)^\pi$	6.72	$\left(1g_{\frac{9}{2}}1g_{\frac{7}{2}}^{-1}\right)^\pi$	96.5
	10.38	$\left(1h_{\frac{11}{2}}1h_{\frac{9}{2}}^{-1}\right)^\nu$	11.11	$\left(1h_{\frac{11}{2}}1h_{\frac{9}{2}}^{-1}\right)^\nu$	98.5	10.53	$\left(1h_{\frac{11}{2}}1h_{\frac{9}{2}}^{-1}\right)^\nu$	10.95	$\left(1h_{\frac{11}{2}}1h_{\frac{9}{2}}^{-1}\right)^\nu$	97.8

TABLE V. The total QRPA transition strengths $\sum B_{M1}^{\text{th.}}$ in μ_N^2 for the Sn isotopes, calculated by using the Skyrme interactions SLy5 and T11 with and without tensor force. The values in the parentheses are obtained in the case of without tensor terms. The calculations are performed in the energy regions which are consistent with the experimental data in Table V of Ref. [32]. The experimental $\sum B_{M1}^{\text{exp.}}$ from Ref. [32] are also shown for comparison. The quenching factors $g_{\text{eff}}/g_{\text{free}}$ for $M1$ resonances in each case are displayed. The calculated quenching factors are also compared to the values of the RQRPA model in Ref. [21].

		^{112}Sn	^{114}Sn	^{116}Sn	^{118}Sn	^{120}Sn	^{124}Sn
$\sum B_{M1}^{\text{th.}}$	Exp.	14.7 ±1.4	19.6 ±1.9	15.6 ±1.3	18.4 ±2.4	15.4 ± 1.4	19.1 ±1.7
	SLy5	27.76(26.84)	24.84(24.58)	23.07(22.78)	22.60(20.42)	25.35(20.36)	25.85(27.41)
	T11	28.86(24.58)	26.11(22.81)	23.94(21.44)	22.37(20.46)	25.88(22.60)	21.88(26.50)
$g_{\text{eff}}/g_{\text{free}}$	SLy5	0.73(0.74)	0.89(0.89)	0.82(0.83)	0.90(0.95)	0.78(0.87)	0.86(0.83)
	T11	0.71(0.77)	0.87(0.93)	0.81(0.85)	0.91(0.95)	0.77(0.83)	0.93(0.85)
	RQRPA	0.80	0.93	0.83	0.89	0.81	0.86

description of the experimental data (details can be found in Ref. [83]). The empirical quenching factor is defined by

$$q = \sqrt{\sum B_{M1}^{\text{exp.}} \Big/ \sum B_{M1}^{\text{th.}}}, \tag{14}$$

where $\sum B_{M1}^{\text{exp.}}$ ($\sum B_{M1}^{\text{th.}}$) is the total experimental (theoretical) transition strength. The extracted quenching factors are about 0.73–0.90 (0.74–0.95) for SLy5 with (without) the tensor terms. Similar values of quenching factors are obtained for T11 with (without) tensor force, and are 0.71–0.93 (0.77–0.95). In Ref. [21], the B($M1$) strengths of $^{112\text{–}120,124}$Sn isotopes were obtained in the framework of relativistic QRPA (RQRPA), and compared with the experimental data. The authors of that work also claimed that quenching factors were needed to reproduce the data. The calculated quenching factors from relativistic EDFs are also listed in Table V and their values, around 0.80–0.93, are similar to those found in our work.

IV. SUMMARY AND PERSPECTIVES

In this paper, we have investigated the magnetic dipole resonances of the even-even $^{112\text{–}120,124}$Sn isotopes, in the framework of the self-consistent Skyrme HF + BCS plus QRPA method. The Skyrme SLy5 and T11 interactions with and without tensor terms are used in the present calculations with a mixed type pairing interaction.

We have also checked other Skyrme sets and we have concluded that the SLy5 and T11 Skyrme interactions, with the tensor terms included, can give a better description of the experimental $M1$ strength distributions of $^{112\text{–}120,124}$Sn [31,32], as compared with others. Taking ^{112}Sn and ^{124}Sn as examples, we have studied the role of tensor force in Hartree-Fock and QRPA response in detail. It is found that magnetic dipole resonances of $^{112\text{–}120,124}$Sn are sensitive to the tensor parameter α_T. A negative α_T leads to reproducing the experimental data. On the other hand, a tensor force with positive α_T, like that of the T15 interaction, gives an opposite contributions to the excitation energies of $M1$ resonances (compared to the case of SLy5 and T11), and the agreement with the experimental data is poorer. This conclusion is not in conflict with that of previous works [33], in which the tensor coupling constant

β is well constrained by the Gamow-Teller and spin-dipole states, while the coupling constant α has a large ambiguity. In fact, the present study of $M1$ strength provides a complimentary constrain on the tensor coupling, the α value is rather well determined, but not the β value. Thus, we definitely need more observables to constrain the tensor terms.

The quenching problem is also discussed in the present work. In our calculations with the tensor terms in the EDFs, we find that a quenching factor of about 0.71–0.93 is needed to reproduce the total experimental transition probabilities for the nuclei we have studied. Without the tensor term, we need quenching factors of more or less similar magnitude.

The calculated results show that low-lying magnetic dipole strength appears in the energy region below 6.0 MeV. It is mainly coming from the neutron configuration $\nu 2d_{5/2} \rightarrow \nu 2d_{3/2}$. However, no clear evidence of low energy $M1$ strength has been found so far in experiments. It would be highly desirable to have further experimental investigations of the $M1$ strength. On the one hand, we would like to confirm or disprove our prediction regarding the low-lying $M1$ strength below 6.0 MeV. On the other hand, there is still some discrepancy between the theoretical results and the experimental results, while the experimental results have some non-negligible error bars at higher energy than 10 MeV. Additional efforts should be envisioned in the future, both on the experimental side and theoretical side. Eventually, it may reveal necessary to further improve the Skyrme energy density functional in the spin-isospin channel.

In Ref. [21], the evolution of magnetic dipole strength of Sn isotopes had been studied in the RQRPA model. The quasi-particle configurations of $M1$ states are essentially the same as those of our calculations; they are mainly the proton configuration $\pi 1g_{9/2} \rightarrow \pi 1g_{7/2}$ and the neutron configurations $\nu 2d_{5/2} \rightarrow \nu 2d_{3/2}$, $\nu 1g_{9/2} \rightarrow \nu 1g_{7/2}$, and $\nu 1h_{11/2} \rightarrow \nu 1h_{9/2}$. The importance of neutron configurations depends on whether the spin-orbit partners are fully occupied or not. The energy dependence of the RQRPA strength is similar to ours, but the energy location of the main $M1$ peak is different because of the different nuclear EDFs adopted. The RQRPA also predicted low-energy $M1$ strengths below 6.0 MeV in ^{112,116}Sn (see Fig. 2 of Ref. [21]), but the strengths are relatively small, which may be due to different occupation probabilities of the orbitals involved in the pygmy states, in the RQRPA calcula-

tion of those nuclei. In Table II of Ref. [21], the total RQRPA transition strengths for $M1$ excitations in $^{112-120,124}$Sn were compared with the experimental data from inelastic proton scattering in Ref. [32]. It has been shown that the calculated values are larger than the experimental data, and in order to reproduce the experimental data, quenching factors of about 0.80–0.93 are needed in RQRPA. These quenching factors are similar to the extracted ones in our case, as shown in Table V.

We should clarify the role of the correlations of beyond mean field. The HF + RPA model has been a very successful model to describe collective states such as low-lying collective states and giant resonances, not only in spherical nuclei but also in deformed nuclei. The width of Gamow-Teller (GT) resonances, and the missing GT strength, cannot be accounted for by the standard mean-field models and the description of these features is much improved by models beyond mean-field like second RPA or particle-vibration coupling models [84–86].

The shift of the excitation energies induced by models beyond mean-field is not completely negligible but less important at the level we discuss in this work. Moreover, the importance of the tensor force was recognized in the splittings of spin-dipole (SD) excitations, already at the RPA level [44]. Therefore, as is done in the present study, the effect of tensor force on the excitation energy of $M1$ state can be discussed at the QRPA level in a solid manner.

ACKNOWLEDGMENTS

[1] M. Harakeh and A. Woude, *Giant Resonances: Fundamental High-frequency Modes of Nuclear Excitation*, Oxford Science Publications (Oxford University Press, Oxford, 2001).

[2] Y. Fujita, B. Rubio, and W. Gelletly, Prog. Part. Nucl. Phys. **66**, 549 (2011).

[3] K. Heyde, P. von Neumann-Cosel, and A. Richter, Rev. Mod. Phys. **82**, 2365 (2010).

[4] A. Richter, Prog. Part. Nucl. Phys. **34**, 261 (1995).

[5] F. Osterfeld, Rev. Mod. Phys. **64**, 491 (1992).

[6] N. Pietralla, G. Rainovski, M. Reese, C. Stahl, T. Beck, J. Beller, C. Romig, and V. Werner, J. Phys.: Conf. Ser. **580**, 012015 (2015).

[7] K. Langanke, G. Martínez-Pinedo, P. von Neumann-Cosel, and A. Richter, Phys. Rev. Lett. **93**, 202501 (2004).

[8] K. Langanke, G. Martínez-Pinedo, B. Müller, H.-T. Janka, A. Marek, W. R. Hix, A. Juodagalvis, and J. M. Sampaio, Phys. Rev. Lett. **100**, 011101 (2008).

[9] H. P. Loens, K. Langanke, G. Martínez-Pinedo, and K. Sieja, Eur. Phys. J. A **48**, 34 (2012).

[10] S. Goriely, S. Hilaire, S. Péru, M. Martini, I. Deloncle, and F. Lechaftois, Phys. Rev. C **94**, 044306 (2016).

[11] S. Goriely and V. Plujko, Phys. Rev. C **99**, 014303 (2019).

[12] P. Vesely, J. Kvasil, V. O. Nesterenko, W. Kleinig, P. G. Reinhard, and V. Y. Ponomarev, Phys. Rev. C **80**, 031302(R) (2009).

[13] V. O. Nesterenko, J. Kvasil, P. Vesely, W. Kleinig, P.-G. Reinhard, and V. Y. Ponomarev, J. Phys. G: Nucl. Part. Phys. **37**, 064034 (2010).

[14] V. Tselyaev, N. Lyutorovich, J. Speth, P.-G. Reinhard, and D. Smirnov, Phys. Rev. C **99**, 064329 (2019).

[15] V. DeDonno, G. Co', C. Maieron, M. Anguiano, A. M. Lallena, and M. Moreno Torres, Phys. Rev. C **79**, 044311 (2009).

[16] G. Co', V. De Donno, M. Anguiano, and A. M. Lallena, Phys. Rev. C **85**, 034323 (2012).

[17] P.-W. Wen and L.-G. Cao, Chin. Phys. Lett. **30**, 052101 (2013).

[18] P.-W. Wen, L.-G. Cao, J. Margueron, and H. Sagawa, Phys. Rev. C **89**, 044311 (2014).

[19] T. Oishi, G. Kružić, and N. Paar, J. Phys. G: Nucl. Part. Phys. **47**, 115106 (2020).

[20] G. Kružić, T. Oishi, D. Vale, and N. Paar, Phys. Rev. C **102**, 044315 (2020).

[21] G. Kružić, T. Oishi, and N. Paar, Phys. Rev. C **103**, 054306 (2021).

[22] S. Y. Chang, Z. H. Wang, Y. F. Niu, and W. H. Long, Phys. Rev. C **105**, 034330 (2022).

[23] B. A. Brown and A. C. Larsen, Phys. Rev. Lett. **113**, 252502 (2014).

[24] R. Schwengner, S. Frauendorf, and B. A. Brown, Phys. Rev. Lett. **118**, 092502 (2017).

[25] K. Sieja, Phys. Rev. C **98**, 064312 (2018).

[26] N. Pietralla, P. von Brentano, and A. Lisetskiy, Prog. Part. Nucl. Phys. **60**, 225 (2008).

[27] H. Pai, T. Beck, J. Beller, R. Beyer, M. Bhike, V. Derya, U. Gayer *et al.*, Phys. Rev. C **93**, 014318 (2016).

[28] H. Matsubara, A. Tamii, H. Nakada, T. Adachi, J. Carter, M. Dozono, H. Fujita, K. Fujita, Y. Fujita, K. Hatanaka *et al.*, Phys. Rev. Lett. **115**, 102501 (2015).

[29] J. Birkhan, H. Matsubara, P. von Neumann-Cosel, N. Pietralla, V. Y. Ponomarev, A. Richter, A. Tamii, and J. Wambach, Phys. Rev. C **93**, 041302(R) (2016).

[30] P. von Neumann-Cosel and A. Tamii, Eur. Phys. J. A **55**, 110 (2019).

[31] T. Hashimoto, A. M. Krumbholz, P.-G. Reinhard, A. Tamii, P. von Neumann-Cosel, T. Adachi, N. Aoi, C. A. Bertulani, H. Fujita, Y. Fujita *et al.*, Phys. Rev. C **92**, 031305(R) (2015).

[32] S. Bassauer, P. von Neumann-Cosel, P.-G. Reinhard, A. Tamii, S. Adachi, C. A. Bertulani, P. Y. Chan, A. DAlessio, H. Fujioka, H. Fujita *et al.*, Phys. Rev. C **102**, 034327 (2020).

[33] H. Sagawa and G. Colò, Prog. Part. Nucl. Phys. **76**, 76 (2014).

[34] T. Otsuka, T. Suzuki, R. Fujimoto, H. Grawe, and Y. Akaishi, Phys. Rev. Lett. **95**, 232502 (2005).

[35] B. A. Brown, T. Duguet, T. Otsuka, D. Abe, and T. Suzuki, Phys. Rev. C **74**, 061303(R) (2006).

[36] G. Colò, H. Sagawa, S. Fracasso, and P. Bortignon, Phys. Lett. B **646**, 227 (2007).

[37] D. M. Brink and F. Stancu, Phys. Rev. C **75**, 064311 (2007).

[38] M. Grasso, Z. Y. Ma, E. Khan, J. Margueron, and N. Van Giai, Phys. Rev. C **76**, 044319 (2007).

[39] W. H. Long, H. Sagawa, N. V. Giai, and J. Meng, Phys. Rev. C **76**, 034314 (2007).

[40] T. Lesinski, M. Bender, K. Bennaceur, T. Duguet, and J. Meyer, Phys. Rev. C **76**, 014312 (2007).

[41] J. M. Dong, W. Zuo, J. Z. Gu, Y. Z. Wang, L. G. Cao, and X. Z. Zhang, Phys. Rev. C **84**, 014303 (2011).

[42] Y. Z. Wang, J. Z. Gu, J. M. Dong, and X. Z. Zhang, Phys. Rev. C **83**, 054305 (2011).

[43] C. L. Bai, H. Q. Zhang, X. Z. Zhang, F. R. Xu, H. Sagawa, and G. Colò, Phys. Rev. C **79**, 041301(R) (2009).

[44] C. L. Bai, H. Q. Zhang, H. Sagawa, X. Z. Zhang, G. Colò, and F. R. Xu, Phys. Rev. Lett. **105**, 072501 (2010).

[45] L.-G. Cao, G. Colò, H. Sagawa, P. F. Bortignon, and L. Sciacchitano, Phys. Rev. C **80**, 064304 (2009).

[46] L.-G. Cao, H. Sagawa, and G. Colò, Phys. Rev. C **83**, 034324 (2011).

[47] F. Minato and C. L. Bai, Phys. Rev. Lett. **110**, 122501 (2013).

[48] V. De Donno, G. Co', M. Anguiano, and A. M. Lallena, Phys. Rev. C **93**, 034320 (2016).

[49] B. Dai, B. S. Hu, Y. Z. Ma, J. G. Li, S. M. Wang, C. W. Johnson, and F. R. Xu, Phys. Rev. C **103**, 064327 (2021).

[50] D. Davesne, M. Martini, K. Bennaceur, and J. Meyer, Phys. Rev. C **80**, 024314 (2009).

[51] A. Pastore, D. Davesne, Y. Lallouet, M. Martini, K. Bennaceur, and J. Meyer, Phys. Rev. C **85**, 054317 (2012).

[52] A. Pastore, M. Martini, V. Buridon, D. Davesne, K. Bennaceur, and J. Meyer, Phys. Rev. C **86**, 044308 (2012).

[53] L. Guo, K. Godbey, and A. S. Umar, Phys. Rev. C **98**, 064607 (2018).

[54] L. Guo, C. Simenel, L. Shi, and C. Yu, Phys. Lett. B **782**, 401 (2018).

[55] P. D. Stevenson, E. B. Suckling, S. Fracasso, M. C. Barton, and A. S. Umar, Phys. Rev. C **93**, 054617 (2016).

[56] R. Alarcon, R. M. Laszewski, and D. S. Dale, Phys. Rev. C **40**, R1097 (1989).

[57] V. Tselyaev, N. Lyutorovich, J. Speth, and P.-G. Reinhard, Phys. Rev. C **102**, 064319 (2020).

[58] L.-G. Cao, S.-S. Zhang, and H. Sagawa, Phys. Rev. C **100**, 054324 (2019).

[59] D. J. Rowe, *Nuclear Collective Motion* (Methuen, London, 1970).

[60] P. Ring and P. Schuck, *The Nuclear Many-Body Problem* (Springer-Verlag, New York, 1980).

[61] A. P. Severyukhin, C. Stoyanov, V. V. Voronov, and N. Van Giai, Phys. Rev. C **66**, 034304 (2002).

[62] G. Colò, L.-G. Cao, N. Van Giai, and L. Capelli, Comput. Phys. Commun. **184**, 142 (2013).

[63] J. Dobaczewski, W. Nazarewicz, and P.-G. Reinhard, Nucl. Phys. A **693**, 361 (2001).

[64] L.-G. Cao, H. Sagawa, and G. Colò, Phys. Rev. C **86**, 054313 (2012).

[65] M. Yamagami, J. Margueron, H. Sagawa, and K. Hagino, Phys. Rev. C **86**, 034333 (2012).

[66] C. A. Bertulani, H. F. Lü, and H. Sagawa, Phys. Rev. C **80**, 027303 (2009).

[67] G. F. Bertsch, C. A. Bertulani, W. Nazarewicz, N. Schunck, and M. V. Stoitsov, Phys. Rev. C **79**, 034306 (2009).

[68] K. Yoshida, Phys. Rev. C **96**, 051302(R) (2017).

[69] E. Chabanat, P. Bonche, P. Haensel, J. Meyer, and R. Schaeffer, Nucl. Phys. A **635**, 231 (1998).

[70] M. Beiner, H. Flocard, N. Van Giai, and P. Quentin, Nucl. Phys. A **238**, 29 (1975).

[71] N. Van Giai and H. Sagawa, Phys. Lett. B **106**, 379 (1981).

[72] J. Bartel, P. Quentin, M. Brack, C. Guet, and H.-B. Hakansson, Nucl. Phys. A **386**, 79 (1982).

[73] J. Dobaczewski, H. Flocard, and J. Treiner, Nucl. Phys. A **422**, 103 (1984).

[74] B. K. Agrawal, S. Shlomo, and V. K. Au, Phys. Rev. C **72**, 014310 (2005).

[75] F. Tondeur, M. Brack, M. Farine, and J. M. Pearson, Nucl. Phys. A **420**, 297 (1984).

[76] F. Tondeur, S. Goriely, J. M. Pearson, and M. Onsi, Phys. Rev. C **62**, 024308 (2000).

[77] S. Goriely, M. Pearson, and F. Tondeur, Nucl. Phys. A **688**, 349 (2001).

[78] S. Köhler, Nucl. Phys. A **258**, 301 (1976).

[79] D. Gambacurta, L. Li, G. Colò, U. Lombardo, N. Van Giai, and W. Zuo, Phys. Rev. C **84**, 024301 (2011).

[80] R. B. Wiringa, V. Fiks, and A. Fabrocini, Phys. Rev. C **38**, 1010 (1988).

[81] W. Zou, G. Colò, Z. Y. Ma, H. Sagawa, and P. F. Bortignon, Phys. Rev. C **77**, 014314 (2008).

[82] M. Grasso and M. Anguiano, Phys. Rev. C **88**, 054328 (2013).

[83] W. Knüpfer, W. Müller, B. C. Metsch, and A. Richter, Nucl. Phys. A **457**, 292 (1986).

[84] Y. F. Niu, G. Colò, E. Vigezzi, C. L. Bai, and H. Sagawa, Phys. Rev. C **94**, 064328 (2016).

[85] D. Gambacurta, M. Grasso, and J. Engel, Phys. Rev. Lett. **125**, 212501 (2020).

[86] M. J. Yang, C. L. Bai, H. Sagawa, and H. Q. Zhang, Phys. Rev. C **106**, 014319 (2022).